J. Fluid Mech. (2005), *vol.* 539, *pp.* 93–112. © 2005 Cambridge University Press
doi:10.1017/S0022112005005768 Printed in the United Kingdom

Average nutrient uptake by a self-propelled unsteady squirmer

By VANESA MAGAR† AND T. J. PEDLEY

Department of Applied Mathematics and Theoretical Physics, Centre for Mathematical Sciences, Cambridge University, Wilberforce Rd, Cambridge CB3 0WA, UK

(Received 1 July 2003 and in revised form 10 January 2005)

We present results for the average mass transfer to a spherical squirmer, a model micro-organism whose surface oscillates tangentially to itself. The surface motion drives a low-Reynolds-number flow which enables the squirmer either to swim relative to the fluid at infinity, at an average speed proportional to a *streaming parameter*, W, or to stir the fluid around it while remaining, on average, at rest (if $W=0$), as represented by a *hovering parameter*, b. We assume that the amplitude of the time-periodic surface distortions is scaled by a dimensionless small parameter ϵ, and consider only high Péclet numbers P – a measure of convection versus diffusion – by setting $P^{-1}=\epsilon^2\gamma$, where γ is a parameter of $O(1)$. It is shown that the average mass concentration distribution satisfies a steady convection–diffusion equation with an effective velocity field that is different from the actual mean velocity field. The model is used to calculate the mass transfer across the surface of the squirmer, measured by the mean Sherwood number Sh.

We find asymptotic solutions for small and large γ and numerical results for the whole range of values. While the large-γ expansions are reproduced well by the numerical results, there is a discrepancy between the two at small γ. We believe this is due to very small recirculation regions, attached to the surface of the squirmer, which make boundary layer theory applicable only when $1/\gamma$ is immense.

For the parameters chosen in this study, results indicate that both hovering and streaming contribute to the mass transfer, although streaming has a greater effect. Also, energy dissipation considerations show that an optimum swimming mode exists, at least at small and large γ, for any given uptake rate. However, other factors have still to be taken into account, and the model realism improved, if we want to make predictions for real aquatic micro-organisms.

1. Introduction

The number of microscopic-plant population explosions, commonly known as algal blooms, keeps increasing in coastal waters. While some blooms may feed and benefit all in the ocean, others can have a negative impact on the environment, on wildlife, and on humans. Processes at the individual level have a strong influence on overall planktonic production, and can determine the properties of ecosystems (Koehl 1989). The amount of nutrient taken up from the water constitutes one of the most important of these processes, because it strongly affects a micro-organism's growth

† Present address: School of Ocean Sciences, University of Wales, Bangor, Menai Bridge, Anglesey LL59 5AB, UK.

https://doi.org/10.1017/S0022112005005768 Published online by Cambridge University Press

and reproduction. However, many factors affecting nutrient uptake still have to be elucidated. In this paper, we will focus on the impact of self-propulsion on the mass transfer to an individual.

Aquatic micro-organisms have developed a variety of self-propelling structures, some of which have been well documented, such as for instance the hair-like organelles, called *cilia*, of ciliated protozoans. Cilia may cover small or large regions of the cell's body. All ciliates beat the cilia to swim, and some species, like the photosynthetic ciliate *Myrionecta rubra* (= *Mesodinium Rubrum*, Krainer & Foissner 1990) for example, beat them very rapidly for short periods of time. *Myrionecta rubra* moves by bursts, or *jumps*. Jakobsen (2001) defines a jump as a "five-fold increase of swimming velocity within the time required to move one bodylength, and a jump path length longer than 10 body lengths". He has observed this swimming behaviour in *Mesodinium Pulex*, a species which has been linked to *M. rubra* but that is in fact different (Crawford 1989), and two other planktonic protists, as an escape response to a syphon flow mimicking the feeding current of some filter feeding copepods. The velocity during the jump was between 100 and 200 bodylengths per second, as observed by several authors (Dale 1987; Crawford 1992; Crawford & Purdie 1992). Other workers observe the velocity to be independent of size (Sleigh & Blake 1977). However, this may depend on the species under consideration (Crawford 1992). Given that the micro-organism responds to hydrodynamical signals, and not to olfactory or visual cues, then the escape response will occur not only in the proximity of predators, but also in (weakly or non-weakly) turbulent flows. This means that micro-organisms in a turbulent environment will jump more frequently than those in calm waters. Observations of *M. Rubra* responses to diurnal flushing from the Southampton estuary support this claim (Crawford & Purdie 1992). Thus, if convection has an effect on the mass transfer, it would be under turbulent conditions and during these bursts of activity when this effect is largest.

In contrast with ciliates, in cyanobacteria the anatomical features responsible for propulsion are not uniquely defined. Several locomotion mechanisms have been proposed according to the strain: some *Oscillatoriaceae* have functional slime-extruding pores and helical fibrils on their surface for screw thread gliding (Hoiczyk & Baumeister 1995; Hoiczyk 2000), while *Synechocystis* (Skerker & Berg 2001) and *Myxococcus* (Wall & Kaiser 1999) use tentacle-like organelles (type IV pili) for social gliding. Recently, some possible locomotive organelles, similar to cilia, have been observed by Samuel, Petersen & Reese (2001) in a *Synechococcus* strain, which led the authors to suggest a locomotive mechanism analogous to that of eukaryotic ciliates.

For simplicity, we will model the micro-organism as a sphere swimming through otherwise still water by means of rapid tangential distortions of its surface, so that a particle on the surface oscillates periodically in time with large frequency σ, and small dimensionless amplitude ϵ. This modelling approach has been used by workers focusing on cyanobacterial propulsion (Stone & Samuel 1996; Ehlers *et al.* 1996). Taylor (1951) and Tuck (1968) focused on infinite sheet models for fish swimming, in which a flexible and thin infinite sheet oscillates to propel itself. Blake (1971*a*) suggested a ciliary propulsion model where the cilia tips are replaced by a moving surface on which travelling waves propagate and induce the propulsive force on each cell, though Lighthill (1952) first analysed the self-propulsion of almost spherical bodies on which surface-travelling waves propagate. In this paper, we use the velocity field calculated by Blake (1971*a*) from the Stokes equations, where the flow is time-dependent but dynamically quasi-steady. However, in contrast with Blake (1971*a*), we restrict attention to surface tangential displacements only and our model

https://doi.org/10.1017/S0022112005005768 Published online by Cambridge University Press

micro-organism, called a *spherical squirmer*, reduces to a sphere of radius a. The velocity field in the frame of reference of the squirmer becomes

$$U_r^* = a\sigma \frac{2B_1}{3}\left(-1+\frac{1}{r^3}\right)P_1(\mu) + a\sigma \sum_{n=2}^{3}\left(\frac{1}{r^{n+2}}-\frac{1}{r^n}\right)B_n P_n(\mu), \tag{1.1}$$

$$U_\mu^* = a\sigma \frac{2B_1}{3}\left(1+\frac{1}{2r^3}\right)V_1(\mu) + a\sigma \sum_{n=2}^{3}\left[\frac{n}{2r^{n+2}}-\left(\frac{n}{2}-1\right)\frac{1}{r^n}\right]B_n V_n(\mu), \tag{1.2}$$

where σ is the principal frequency of oscillation, V_n is defined as

$$V_n = \frac{2\sqrt{1-\mu^2}}{n(n+1)}\,P_n'(\mu),$$

with $\mu = \cos\theta$ and P_n the Legendre polynomial of order n. Here r ($r = r^*/a$) and θ are dimensionless spherical polar coordinates. We also have assumed that only the first three coefficients in the expansions (1.1) and (1.2) are non-zero. The parameters B_1, B_2 and B_3 are functions of time and they represent a wave of tangential displacements moving around the surface of the micro-organism. In fact, a material point, initially at θ_0, will, at dimensionless time t ($t = \sigma t^*$), be in the position

$$\theta = \theta_0 + \epsilon \sum_{n=1}^{3} \beta_n(t) V_n(\cos\theta_0) = \theta_0 + \epsilon\{(b_1 V_1 + b_3 V_3)\sin t + b_2 V_2 \cos t\}, \tag{1.3}$$

where we have chosen the functions β_n as oscillatory functions of time. The small parameter ϵ gives a measure of the amplitude of the wave. The normalized distance $(\theta-\theta_0)/\epsilon$ is the sum of three standing waves, with two extrema when $t \neq \frac{1}{2}\pi(\mathrm{mod}\ \pi)$, at $\theta = \frac{1}{4}\pi$ and $\theta = \frac{3}{4}\pi$, or three when $t = \frac{1}{2}\pi(\mathrm{mod}\ \pi)$; the nodal points are at 0 and π.

Now, using the definition and the Taylor expansion of the tangential velocity at the surface, and the orthogonality relationship for the associated Legendre polynomials, Blake (1971*b*) deduced that

$$B_n = \epsilon\dot{\beta}_n - \frac{\epsilon^2}{8} n(n+1)(2n+1) \sum_{m,k=1}^{3} \beta_m \dot{\beta}_k \int_0^\pi V_n V_m \frac{\mathrm{d}V_k}{\mathrm{d}\theta}\,\sin\theta\,\mathrm{d}\theta; \tag{1.4}$$

see also Brennen (1974). The integrals in the above equation may be determined explicitly, leading to

$$B_n = \epsilon\dot{\beta}_n + \epsilon^2 \sum_{m=1}^{m=3}\sum_{k=1}^{k=3} c_{nmk}\beta_m\dot{\beta}_k, \tag{1.5}$$

where c_{nmk} is known; it becomes clear that B_n has a term proportional to $\dot{\beta}_n$, and terms proportional to the products $\beta_m\dot{\beta}_k$. Thus, the velocity field is of the general form

$$U_r^* = a\epsilon\sigma u_1(r,\mu,t) + a\epsilon^2\sigma[u_0(r,\mu) + u_2(r,\mu,t)], \tag{1.6}$$

$$U_\mu^* = a\epsilon\sigma v_1(r,\mu,t) + a\epsilon^2\sigma[v_0(r,\mu) + v_2(r,\mu,t)]. \tag{1.7}$$

Thus, the normalized flow,

$$\boldsymbol{U} = \frac{\boldsymbol{U}^*}{a\sigma\epsilon} = \boldsymbol{u}_1(r,\mu,t) + \epsilon[\boldsymbol{u}_0(r,\mu) + \boldsymbol{u}_2(r,\mu,t)], \tag{1.8}$$

https://doi.org/10.1017/S0022112005005768 Published online by Cambridge University Press

is composed of (*a*) a steady part, $\epsilon \boldsymbol{u}_0 = \epsilon(u_0, v_0)$, of order ϵ, (*b*) an oscillatory component $\boldsymbol{u}_1 = (u_1, v_1)$, of order 1, and of the same frequency as the fundamental frequency of the surface oscillations, and (*c*) the component $\epsilon \boldsymbol{u}_2 = \epsilon(u_2, v_2)$, of order ϵ, which oscillates at twice the fundamental frequency. The oscillatory parts of the velocity field can therefore be written as

$$\boldsymbol{u}_j = (u_j, v_j) = \mathrm{Re}[\tilde{\boldsymbol{u}}_j \exp(\mathrm{i}jt)]; \tag{1.9}$$

the real and imaginary parts of $\tilde{\boldsymbol{u}}_j$ are given explicitly in Appendix A. Solution (1.8) may be thought of as the first two terms of an expansion in ϵ of the velocity field, as explained by Brennen (1974). As stated above, we are restricting our attention to these terms, mainly to simplify the analysis and see the effect on the mass transfer. This model is idealized in many ways, but relaxing individual idealizations, such as using a higher wavenumber, would increase the realism only slightly.

The basic hypothesis of this work is that the squirming motions stir up the fluid near the sphere and, if sufficiently vigorous, will enhance the absorption of nutrients by the cells. It turns out that 'sufficient vigour' requires that we set the Péclet number to $P^{-1} = \gamma\epsilon^2$, with γ of order 1. We calculate the averages, over a time cycle, of the concentration field and the total mass transfer to the squirmer. The average concentration field equation is a steady advection–diffusion equation, as for a steady squirmer (Magar, Goto & Pedley 2003), except that now the effective steady velocity field $\boldsymbol{A}$ is different from the steady part $\boldsymbol{u}_0$ of the actual velocity field. Adopting an Eulerian point of view, (A_r, A_θ) may be written as a *hovering* velocity characterized by a parameter b, and a *streaming* velocity proportional to a parameter W (see below). *Browsing* is the term used for motion which combines the two regimes. Asymptotic solutions for small and large γ are obtained, and numerical results determined for the whole range of values of γ.

2. The mass transfer equation

The concentration of dissolved nutrients C^*, changes in time subject to the flow field (1.6) and (1.7), and to random motions quantified by the diffusivity D,

$$C^*_{t^*} + \boldsymbol{U}^* \cdot \nabla^* C^* = D\nabla^{*2} C^*. \tag{2.1}$$

With C^*_∞ the concentration at infinity, and C^*_0 the concentration at the surface of the micro-organism, the scalings $r^* = ar$, $t^* = t/\sigma$, $\boldsymbol{U}^* = a\epsilon\sigma\boldsymbol{U}$, and $C^* = (C^*_0 - C^*_\infty)C + C^*_\infty$, lead to the transport equation

$$C_t + \epsilon \boldsymbol{U} \cdot \nabla C = P^{-1}\nabla^2 C. \tag{2.2}$$

The quantity $P = a^2\sigma/D$, defined as the *Péclet number*, measures the relative importance of advection versus diffusion. Realistic values for P are small to moderately large – $O(100)$, say – for dissolved nutrients. For instance, using the data reported by Crawford & Purdie (1992), who have found escape velocities for *M. Rubra* larger than 8 mm s^{-1}, or 200 bodylengths per second (corresponding to a bodylength of 40 μm), and taking 10^{-3} mm^2 s^{-1} as a typical value for the diffusion coefficient of solutes in water (Ghiu, Carnahan & Barger 2002), we find that the Péclet number has a value of 320. P would be much smaller for uptake by bacteria, say, but could be larger for larger ciliates or for uptake of very large molecules or colloidal particles such as viruses, for which D is very small. The most interesting effects occur for large P, so we set $P^{-1} = \gamma\epsilon^2$, where ϵ is the amplitude of oscillation

https://doi.org/10.1017/S0022112005005768 Published online by Cambridge University Press

and γ is formally of $O(1)$, and then consider both large and small γ, for it is unclear what physical values would be appropriate for the amplitude of oscillations.

Since we are assuming that ϵ is a small parameter, we cannot neglect the temporal variations of the concentration field when solving equation (2.2), even at large Péclet numbers. However, we can compute the time-averaged concentration field for and mass transfer rate to the squirming sphere, from equation (2.2), with the boundary conditions $C=1$ on the surface of the micro-organism, and $C=0$ at infinity.

A measure of the mass transfer rate is given by the Sherwood number, defined as

$$Sh = \int_{-1}^{1} \left(\frac{\partial C}{\partial r} \right)_{r=1} \mathrm{d}\mu, \tag{2.3}$$

but since we will determine the average nutrient absorption only, C in equation (2.3) is in fact the average concentration field over a time cycle.

3. Solution for P large

With $P=(\epsilon^2\gamma)^{-1}$, we try a regular expansion

$$C = C_0 + \epsilon C_1 + \epsilon^2 C_2 + \ldots. \tag{3.1}$$

Substituting this expansion, together with the complete velocity field, into the mass transfer equation (2.2), we deduce at once that C_0 is independent of time.

Next, the $O(\epsilon)$ equation gives

$$\frac{\partial C_1}{\partial t} = -\boldsymbol{u}_1 \cdot \nabla C_0 = -\frac{1}{2}[\tilde{\boldsymbol{u}}_1 \exp(\mathrm{i}t) + \bar{\tilde{\boldsymbol{u}}}_1 \exp(-\mathrm{i}t)] \cdot \nabla C_0, \tag{3.2}$$

where $\boldsymbol{u}_1$ was defined earlier – see equations (1.6) and (1.7) – and an overbar means complex conjugate. Integrating gives

$$C_1 = \bar{C}_1(r,\theta) + \frac{\mathrm{i}}{2}[\tilde{\boldsymbol{u}}_1 \exp(\mathrm{i}t) - \bar{\tilde{\boldsymbol{u}}}_1 \exp(-\mathrm{i}t)] \cdot \nabla C_0; \tag{3.3}$$

thus, C_1 is the sum of an unknown time-independent function, and of two terms oscillating in time at the fundamental frequency of oscillation of the surface.

Then, at $O(\epsilon^2)$ we have

$$\frac{\partial C_2}{\partial t} + \boldsymbol{u}_1 \cdot \nabla C_1 + (\boldsymbol{u}_0 + \boldsymbol{u}_2) \cdot \nabla C_0 = \gamma \nabla^2 C_0. \tag{3.4}$$

Finally, we take the time average of equation (3.4), using equation (3.2), and obtain a steady convection–diffusion equation for C_0, of the form

$$\boldsymbol{A} \cdot \nabla C_0 = \gamma \nabla^2 C_0, \tag{3.5}$$

where the effective velocity field $\boldsymbol{A}$ is,

$$\boldsymbol{A} = \tfrac{1}{2}\mathrm{Im}(\tilde{\boldsymbol{u}}_1 \cdot \nabla \bar{\tilde{\boldsymbol{u}}}_1) + \boldsymbol{u}_0. \tag{3.6}$$

It should be noted that $\boldsymbol{A}$ is not the same as the real mean velocity field $\boldsymbol{u}_0$. Appendix B summarizes the main steps of the calculation of $\boldsymbol{A}$.

It can be seen that (3.5) is the steady mass transfer equation, as analysed for steady squirmers by Magar *et al.* (2003), but with an effective velocity field instead of the actual steady squirming velocity of the model described in that paper, and with $1/\gamma$ in the role of the Péclet number.

Since all the velocity fields depend on the products $b_1 b_2$ and $b_2 b_3$, we choose to express $\boldsymbol{A}$ in terms of a parameter b defined as $b_1 b_2$, and a parameter W proportional

https://doi.org/10.1017/S0022112005005768 Published online by Cambridge University Press

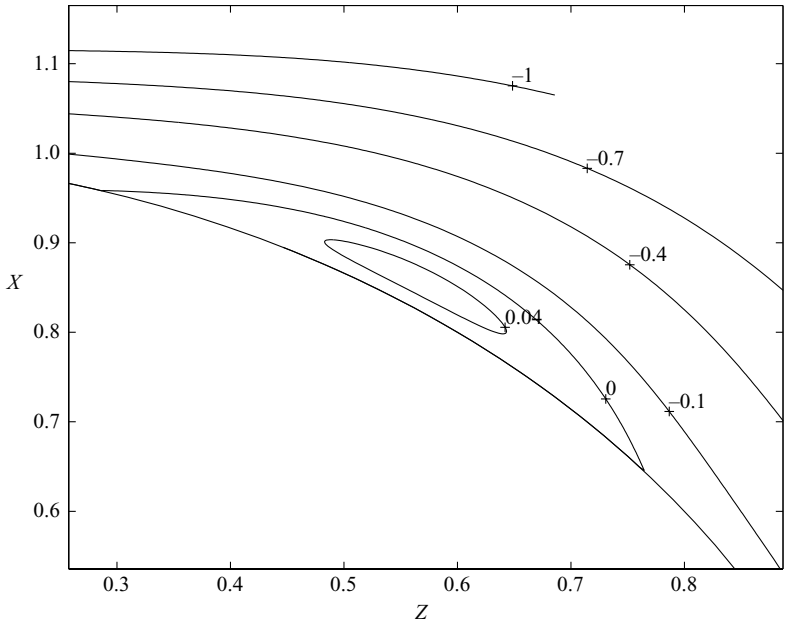


FIGURE 1. Close-up of the recirculation region when $b = 60$ and $W = 1$.

to the mean with respect to time of the cell's swimming velocity, which is given by Blake (1971*b*). With the simplifications assumed in this work, W reduces to $4b_2(-b_1/3 + b_3/7)/5$. We call b the *hovering* parameter because when $W = 0$ and $b \neq 0$ there is stirring, but no mean swimming speed, while W is designated as a *streaming* parameter. Finally, *browsing* refers to the general mode of locomotion, that is, the mode where the micro-organism both hovers and streams to propel itself through the water and stir the nutrients.

It is of interest to note that, unlike the actual mean velocity field, the tangential velocity A_θ vanishes at six points over the surface in the upper hemisphere of the squirmer, at values of $\mu_0 = \cos\theta_0$ which are roots of the polynomial $(\mu_0^2 - 1)(21\mu_0^4 - 14\mu_0^2 + 1)$ – see Appendix A. Thus, for any value of b or W, there is a tiny toroidal recirculation region, attached to the surface of the micro-organism, as shown in figure 1 for values of $b = 60$ and $W = 1$. These recirculation regions are absent in streamline contours of the steady flow field $\boldsymbol{u}_0$. While it is clear that near the micro-organism the effect of the averaged term has an important influence on the streamlines, in the far field the steady flow $\boldsymbol{u}_0$ dominates the fluid motion. For the example in figure 1 the flow $\boldsymbol{A}$ flattens the streamlines near the region above the micro-organism, but the effect close to the cell's surface depends on the values of b and W chosen.

4. Asymptotic expansions for small and large $1/\gamma$

As indicated by Magar *et al.* (2003), equation (3.5) may be solved asymptotically for both small and large values of the parameter $1/\gamma$, which is a measure of the effective Péclet number. The determination of the Sherwood number for small $1/\gamma$ is straightforward if one follows a procedure similar to that developed by Acrivos &

https://doi.org/10.1017/S0022112005005768 Published online by Cambridge University Press

Taylor (1962), and the expansion of Sh to second order,

$$Sh = 2 + \frac{W}{\gamma} + \frac{1}{\gamma^2}(-0.3314W^2 + 1.6757 \times 10^{-2}Wb + 8.2834 \times 10^{-5}b^2), \tag{4.1}$$

shows that the streaming part of the flow has a greater impact on the nutrient uptake than the hovering part. In fact, to first order the nutrient distribution and uptake are completely determined by the magnitude of the mean swimming speed.

In the large-$1/\gamma$ limit, when convection dominates the distribution of nutrients, the concentration contours follow closely the effective streamlines. Here the concentration gradients are very large close to the surface of the squirmer, leading to the formation of a concentration boundary layer in the vicinity of the cell surface. In this region the coordinate system is approximately orthogonal, with a local variable $Y = (r-1)/\gamma^{1/2}$ chosen so that, at large $1/\gamma$ and close to the squirmer's membrane, convection and diffusion are both important, and equation (3.5) simplifies to

$$\frac{\partial^2 C}{\partial Y^2} = -Yf'(\mu)\frac{\partial C}{\partial Y} + f(\mu)\frac{\partial C}{\partial \mu}, \tag{4.2}$$

where $f(\mu) = (1/9)(b/3 + 5W/4)(1-\mu^2)^{1/2}P_5^1(\mu)$, $P_5^1(\mu)$ being the Legendre function of first degree and fifth order. Equation (4.2) above holds if the gradient of the concentration is linear in the boundary layer. If the effective velocity A_θ vanished in some region on the surface of the sphere, then a scaling of the order of $\gamma^{1/3}$ would be expected there. However, the no-slip condition is satisfied only at six stagnation points on the surface (see below) so such a region does not exist.

A similarity solution $C = \mathrm{erfc}[Y/g(\mu)]$ will exist if g is a solution of $f'g^2 + \frac{1}{2}f(g^2)' = \beta$, where β is an arbitrary constant; this leads to a function of the form

$$g = \frac{1}{f}\left\{\alpha + \beta\int^{\mu} f(\rho)\,\mathrm{d}\rho\right\}^{1/2}, \tag{4.3}$$

with α a constant. Thus,

$$g(\mu) = \sqrt{\frac{96}{5(b/3+5W/4)}}\frac{(k + 3\mu^7 - 7\mu^5 + 5\mu^3 - \mu)^{1/2}}{|(\mu^2-1)(21\mu^4 - 14\mu^2 + 1)|}, \tag{4.4}$$

where k depends on α and β. We propose that g must be bounded at any stagnation point at which the flow impinges on the squirmer surface. There are three such points: at $\mu_{inf} = 1$, 0.2852 and -0.7650. Accordingly, the flow streamlines separate at the points $\mu_{sup} = 0$, 0.7650 and -0.2852. Now, given that the boundary layer thickness is of order $\gamma^{1/2}$, the Sherwood number is proportional to $\gamma^{-1/2}$, and one may easily relate the constant of proportionality, c say, to the function g given by (4.4) above (Leal 1992), and conclude that

$$c = \sqrt{\frac{5(b/3+5W/4)}{6\pi}}\sum_{\mu_{inf}}[h(\mu_{sup}) - h(\mu_{inf})]^{1/2}, \tag{4.5}$$

with $h(\mu) = 3\mu^7 - 7\mu^5 + 5\mu^3 - \mu$. The sum is over the five surface intervals between the six stagnation points on the upper hemisphere. Adding all contributions, we then obtain at leading order,

$$Sh = 1.182\sqrt{\frac{b/3+5W/4}{\gamma}}, \tag{4.6}$$

https://doi.org/10.1017/S0022112005005768 Published online by Cambridge University Press

which shows that for large $1/\gamma$ both swimming modes are important, although the streaming flow still affects the nutrient distribution to a somewhat larger extent than the hovering. Finally, the example portrayed in figure 1 indicates a maximal thickness of the recirculation region of around 0.08, and since the boundary layer thickness is of the order of $\gamma^{1/2}$ for small γ, for the boundary layer to be thin enough we require that $\gamma^{1/2} \ll 0.08$, say

$$\gamma^{1/2} \approx 0.005;$$

thus, to reproduce the asymptotic behaviour we would need to consider values of $1/\gamma$ around 40 000. This is beyond the scope of our computations.

5. Numerical procedures

No analytical solution is available when $1/\gamma$ takes intermediate values; for that range, therefore, we have computed the Sherwood number using several techniques. For a hovering micro-organism, we considered a Legendre polynomial spectral method (in θ) such as that used by Magar *et al.* (2003), with finite-difference discretization (in r), but solved iteratively with two different iteration schemes: the generalized minimal residual (GMRES) method (Saad & Schultz 1986), or the biconjugate gradient stabilized (BiCGSTAB) algorithm. For cases when W is non-zero, we used instead a finite-volume code, also described in Magar *et al.* (2003); in addition, for streaming micro-organisms, we computed the concentration distribution using an adaptive finite-difference algorithm (Blom, Trompert & Verwer 1996). The adaptive algorithm uses the Method of Lines to reduce equation (3.5) to a system of ordinary differential equations, which is discretized by second-order finite differences and solved iteratively using the BiCGSTAB method. Finally, the system of differential algebraic equations is solved implicitly using a time-integrator with variable step sizes. The reason for using so many different techniques is that the results, at large values of $1/\gamma$, did not agree with the asymptotic solution and further confirmation was needed.

In all the schemes, we used the radial variable $\xi = \ln r$, so that the grid was finer close to the sphere surface and coarser in the far field. In the finite-volume code, the grid size was adjusted according to the value of $1/\gamma$, so that there were at least five grid points, in the radial direction, inside the boundary layer predicted by the theory (see § 4). For $b = 0$ and W/γ up to 200, for instance, it is sufficient to have the radial grid size of the order of 10^{-3}, or an angular grid size around 0.3°.

On the other hand, the adaptive scheme starts with a coarse grid, and this grid is refined (up to a level chosen by the code user) by bisection in every coordinate direction. In regions of steep gradients in space, the convection–diffusion equation is solved in a series of nested grids, and all the points computed are afterwards used in the solution. This practical feature keeps the amount of computer space and computer time to a minimum, and constitutes a clear advantage of the adaptive code over the finite-volume one. Another advantage of this algorithm over the finite-volume code is that the former is vectorized, originally for the Cray YMP (Blom *et al.* 1996), but we modified it to have the appropriate machine constants for machines with IEEE arithmetic, such as IBM PCs, and used the vectorizer of the Intel Fortran Compiler. So, the adaptive code is preferable in terms of speed and memory storage.

In the finite-volume and adaptive codes, we add the term $\partial \bar{C}_0/\partial t$, to the right-hand side of equation (3.5), that is, we convert it into an unsteady convection–diffusion equation, and determine then the steady state. The computations start impulsively at $t = 0$ in both algorithms; that is, we assume that $C = 1$ at the surface (which has been

https://doi.org/10.1017/S0022112005005768 Published online by Cambridge University Press

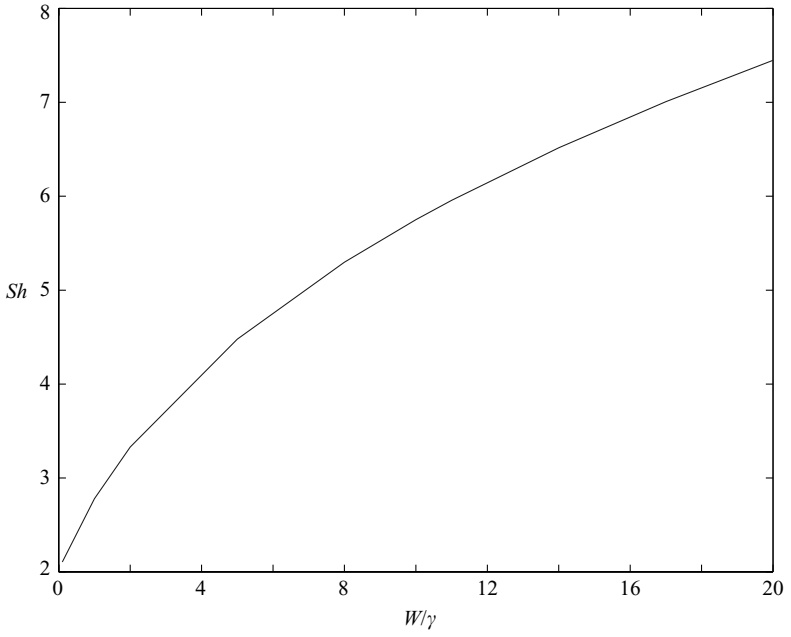


FIGURE 2. *Sh* vs. W/γ for W/γ up to 20, for streaming squirmers ($b=0$), from the finite-volume code.

reduced to the point $\xi=0$), and $C=0$ elsewhere. Also, the nutrient concentration is set to zero at a sufficiently large value ξ_{max} of ξ – see Magar *et al.* (2003) for a discussion on the validity of this approximation. Finally, the axisymmetric flow condition implies that there is no flux of nutrients across the axis of symmetry $\theta_0=0$. Other than the similarities pointed out, the two codes follow different numerical techniques, but both should give comparable results for the Sherwood number as a function of the parameters $1/\gamma$, b, and W.

6. Results and discussion

6.1. *Streaming micro-organisms*

For squirmers streaming through the water ($b=0$), we determined the Sherwood number for values of W/γ larger than 0.2, and compared it to the asymptotic behaviour when possible. When W/γ is small, the code and the expansion (4.1) give comparable results for W/γ up to approximately 0.5; for larger values, only numerical techniques are available. Results for the *Sh* vs. W/γ relationship, up to $W/\gamma=20$, are shown in figure 2.

For values of W/γ between 20 and 100, both codes suggested that *Sh* was accurately proportional to a power of W/γ. Using the finite-volume method (FVM), this relationship was of the form

$$Sh = 2.444(W/\gamma)^{0.372}, \tag{6.1}$$

while the adaptive finite-differences algorithm gave

$$Sh = 2.445(W/\gamma)^{0.373}, \tag{6.2}$$

using a completely different procedure. Thus, expressions (6.1) and (6.2) can be taken to be reliable; the discrepancy with the asymptotic expansion (4.6) at large W/γ may

https://doi.org/10.1017/S0022112005005768 Published online by Cambridge University Press

therefore be attributed to the fact that the values of W/γ for which (6.1) and (6.2) are valid are too low for large-W/γ asymptotics to apply.

It remained inconclusive whether the numerical schemes produced an asymptotic behaviour of the form $Sh \propto (W/\gamma)^{0.5}$ for values of W/γ much larger than 100, because we cannot claim accuracy of the computations for such parameter values. However, if we fit a curve to the results on a log-log plot, its slope increases gradually as W/γ increases, but is still smaller that 0.5.

6.2. *Hovering micro-organisms*

In this case there is no uniform flow at infinity ($W = 0$) and both the velocity field and the Sherwood number are functions of b/γ (see Appendix A). As stated in § 5, the results were obtained using the Legendre polynomial method with the iterative scheme developed by Saad & Schultz (1986). For b/γ up to unity, the results were best approximated by

$$Sh = 2.00007 + 0.0000829\left(\frac{b}{\gamma}\right)^2. \tag{6.3}$$

Comparing this with (4.1), we see that the agreement is excellent. In fact, equation (6.3) approximates the numerical results with good accuracy for b/γ up to 100 (the relative error is smaller than 1 %).

For larger b/γ, only results up to $b/\gamma = 395$ could be obtained, before the computation broke down because the number of non-zero entries in the preconditioning decomposition became too large. The functional relationship to which the results seem to tend as b/γ increases,

$$Sh = 0.285\left(\frac{b}{\gamma}\right)^{0.472}, \tag{6.4}$$

is again not the expected asymptotic behaviour given by (4.6). However, the relative error between the power 0.472 and the expected 0.5 power is less than for a streaming squirmer. Again, the discrepancy between numerical and analytical results is thought to be due to the presence of the toroidal recirculation regions mentioned above.

Notice the combined effect of the swimming mechanism and the Péclet number, on the nutrient uptake by the swimmer: if b is large then the Sherwood number remains large even when $1/\gamma = O(1)$, so the effect of swimming on the nutrient uptake is significant. However, our model is too idealized for practical applications and this can be only a qualitative conclusion.

6.3. *Browsing micro-organisms*

Lastly, we consider the most general form of swimming motion, that is, one which combines both streaming and hovering. In this case, we analyse the problem in terms of the parameter $1/\gamma$. The results for small $1/\gamma$ (up to 4.5) were obtained using the Legendre polynomial expansion method, and the agreement with (4.1) was good to within 1 % for $1/\gamma$ up to 0.6. Thereafter the numerical data start to diverge.

For intermediate and large $1/\gamma$, the flow field strongly influences the nutrient concentration distribution at the back of the squirmer, as figure 3 shows. Also, increasing W had a considerable effect on the nutrient uptake. For instance, if $1/\gamma = 200$ and $b = 60$, the Sherwood number is 20 % larger when $W = 10$ than when $W = 1$. This suggests that the swimmer may be more likely to stream rapidly when browsing. However, hovering also has a positive effect, for the Sherwood number is smaller if $b = 0$ and $W = 10$ than when $b = 60$ and $W = 10$. Thus, in terms of uptake

https://doi.org/10.1017/S0022112005005768 Published online by Cambridge University Press

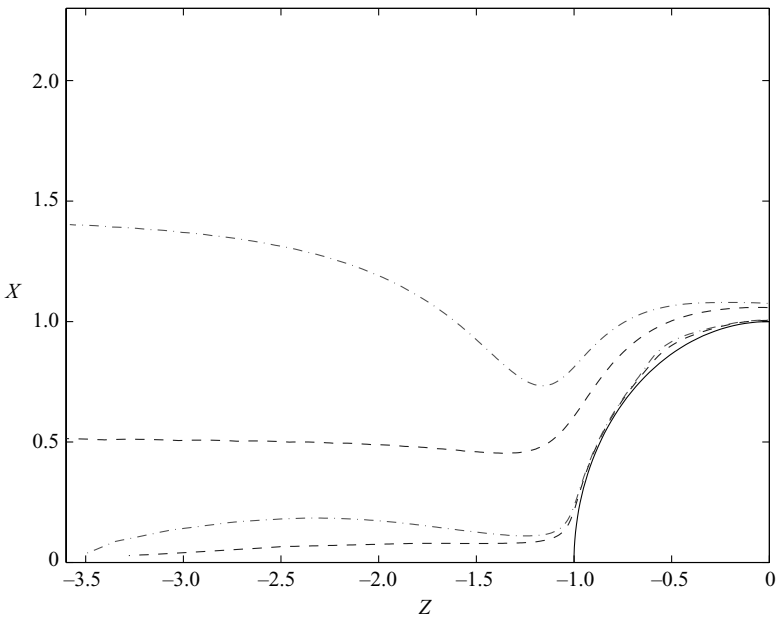


FIGURE 3. Concentration contours $C = 0.05$ (upper curves) and $C = 0.85$ (lower curves), for $b = 60$, $W = 1$ (dash-dotted lines) and $b = 60$, $W = 10$ (dashed lines). For both values of W, the parameter $1/\gamma$ was set to 110.

rate, the micro-organisms will try to hover and stream at the highest possible speed. However, this might not be so advantageous in terms of energy requirements, as investigated in the next section.

7. Energy dissipation

The total rate of energy dissipation in the fluid, as a result of the squirming motion, is of the same magnitude and opposite sign as the total rate of working E by the fluid on the surface, calculated by Blake (1971*b*). A suitably modified version of his expression gives

$$E = \frac{16\pi\mu}{3}B_1^2 + \frac{8\pi\mu}{3}B_2^2 + \frac{4\pi\mu}{3}B_3^2. \tag{7.1}$$

The average rate of working $\langle E\rangle$, over a time cycle, is found by taking the real part of each B_n, squaring it, integrating the result over a time period and dividing the final expression by the time period. In order to express $\langle E\rangle$ in terms of the hovering and streaming parameters, note that b and W depend on b_2 in the same way. Thus, we assume that $b_2 = 1$. Now, define a non-dimensional energy dissipation as $\tilde{E}(\epsilon, b, W) = \langle 3E/(4\pi\mu)\rangle$; using the definitions of b and W, we find that

$$\tilde{E}(\epsilon, b, W) = 1 + W^2\left(\frac{1225}{32} + \frac{245}{12}\frac{b}{W} + \frac{85}{18}\frac{b^2}{W^2}\right)$$
$$+ 2\epsilon\left[W^2\left(\frac{175}{64} + \frac{125}{24}\frac{b}{W} + \frac{25}{36}\frac{b^2}{W^2}\right) - \frac{1}{14}\right]^2 + \epsilon^2 W^2\left(\frac{505}{48} + \frac{5}{18}\frac{b}{W} + \frac{25}{27}\frac{b^2}{W^2}\right). \tag{7.2}$$

Consequently, the energy dissipation depends on the characteristics of the swimming mechanism, but (of course) not on the Péclet number.

https://doi.org/10.1017/S0022112005005768 Published online by Cambridge University Press

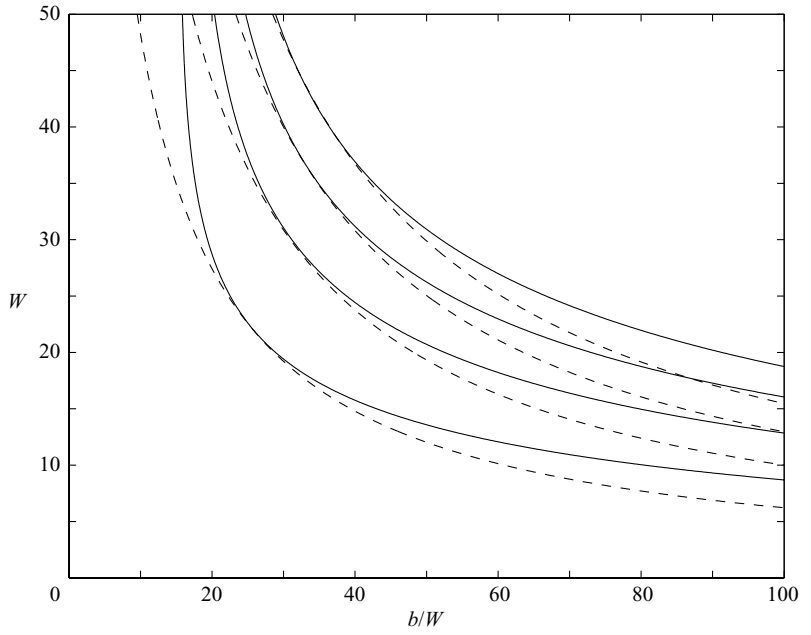


FIGURE 4. Sherwood number contour plots (solid lines) and E contour plots (dashed lines) when $1/\gamma = 0.15$. E increases in the direction of increasing b/W and increasing W. The four pairs of contours plotted here correspond (from bottom to top) to $(Sh-2, E) = (5, 4.2\times10^{15})$, $(10, 2.8\times10^{16})$, $(15, 7.9\times10^{16})$ and $(20, 1.6\times10^{17})$ – the values of E are the approximate constrained minima for the values of Sh shown here.

As given in (7.2), we see that the energy dissipation is a second-order polynomial in the amplitude ϵ of the oscillations, and that each coefficient of the polynomial has the same qualitative behaviour (for positive values of W and b): they increase as either W or b increases. Therefore, we may take a particular value of ϵ (here, $\epsilon = 0.1$) without fear of distorting the qualitative results. If we calculate E for the three pairs of (b, W) considered at the end of § 6, we find that $E(0.1, 0, 10) = 1.88\times10^4$, whereas $E(0.1, 60, 1) = 1.60\times10^6$ and $E(0.1, 60, 10) = 6.99\times10^6$. Therefore when $b = 0$ and $W = 10$ the organism dissipates less energy, but with this mode it also absorbs less nutrient. In practice we might expect it to make a compromise and choose the self-propulsion mode with least energy dissipation, for a given Sherwood number.

Therefore, one should be able to find b/W and W such that E is minimum, for given Sh and $1/\gamma$. When $1/\gamma$ is small this extremum, if it exists, can be determined using equation (4.1) for the Sherwood number as a constraint. However, it is simpler to analyse the problem graphically and use (4.1) to plot Sherwood number contours instead. The same applies to large $1/\gamma$, assuming the asymptotic expression (4.6) for, say, $1/\gamma \geqslant 1000$.

Figures 4 and 5 show these contours (solid lines) for $1/\gamma = 0.15$ and for $1/\gamma = 1000$. It is of interest to note that Sh increases in the directions both of increasing b/W and of increasing W. If we construct a contour plot of Sh, then for $1/\gamma = 0.15$ we can find a curve $E =$ constant (dotted lines) which touches the Sh contour plot at only one point; this corresponds to a minimum of the energy dissipation for that uptake rate, since curves with larger E intersect the chosen Sherwood number contour at more than one point. At large $1/\gamma$ ($= 1000$), however, this minimum dissipation for given uptake rate occurs at $b = 0$ (figure 5). We conclude that, in the ranges of the Sherwood

https://doi.org/10.1017/S0022112005005768 Published online by Cambridge University Press

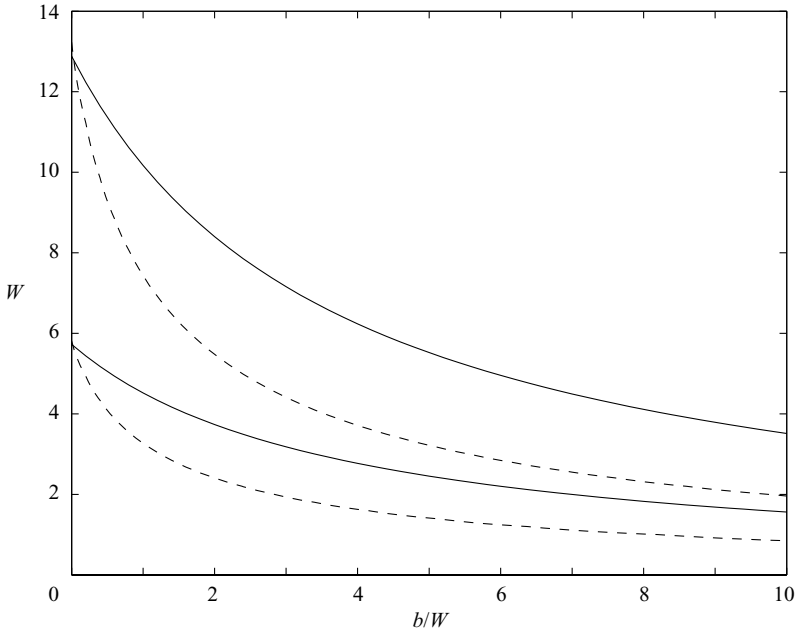


FIGURE 5. Sherwood number contour plots (solid lines) and E contour plots (dashed lines) when $1/\gamma = 1000$. Same comments as for the previous figure apply at large $1/\gamma$. Note, however, that the energy minima occur for streaming motion, i.e. $b = 0$. The two pairs of contours are $(Sh, E) = (0.1, 4.3 \times 10^8)$ and $(0.15, 1.15 \times 10^{10})$.

number where the asymptotic expansions are valid, there is an optimal swimming motion which minimizes the energy dissipation for a given Sherwood number, and a swimming micro-organism may be expected to choose that swimming mode, other things being equal. However, other factors, such as mate searching or predation, may make other swimming modes more appropriate in practice.

8. On an alternative boundary condition

We now consider an alternative boundary condition representing a case in which nutrients are taken up by the micro-organism, and are consumed at a given rate per unit volume, as well as diffusing within it. This internal consumption limits the nutrient uptake rate when there is little resistance to mass transfer in the fluid, i.e. when the concentration boundary layer is thin, i.e. when γ^{-1} is large. This formulation was considered by Magar *et al.* (2003) for steady squirmers; the nutrient concentration inside the cell, C_{cell}, satisfies

$$\frac{\partial C_{cell}}{\partial t} + k^2 C_{cell} = D_{cell} \nabla^2 C_{cell}, \tag{8.1}$$

with D_{cell} the nutrient diffusivity inside the cell, and k the nutrient absorption coefficient. Now, given that the concentration outside the cell is a regular expansion of the amplitude of oscillation ϵ, we assume that $C_{cell} = \sum_{n=0}^{\infty} \epsilon^n (C_{cell})_n$; thus, all the $(C_{cell})_n$ are solutions of equation (8.1).

https://doi.org/10.1017/S0022112005005768 Published online by Cambridge University Press

Also, since we are interested only in the average nutrient uptake, we may consider the steady solution for the nutrient distribution inside the cell. Thus, $(C_{cell})_n$ satisfies

$$\kappa^2(C_{cell})_n = \nabla^2(C_{cell})_n, \tag{8.2}$$

with $\kappa = ak/\sqrt{D_{cell}}$, and the average concentration distribution outside the micro-organism is still described by equation (3.5), except that here we take the dimensionless concentration $C_0 = C^*/C^*_\infty$. The boundary conditions,

$$C_0 \to 1 \text{ as } r \to \infty, \text{ and } \frac{\partial C_0}{\partial r} = D'\frac{\partial C_{cell}}{\partial r} = \beta'(C_0 - C_{cell}) \quad \text{when } r \to \infty, \tag{8.3}$$

with $\beta' = \beta/D$ and $D' = D_{cell}/D$, and equations (3.5) and (8.2), are all four of the same form as those analysed by Magar *et al.* (2003), the only difference being the effective external velocity field $\boldsymbol{A}$.

At small values of $1/\gamma$, the solution is found in the same way as in the above paper. The zeroth-order solution is spherically symmetric both inside and outside the micro-organism, and the solution was found in the form

$$C_{00} = 1 - \frac{\lambda}{r}, \ (C_{cell})_0 = \frac{\kappa\lambda}{\kappa\cosh\kappa - \sinh\kappa}\frac{\sinh(\kappa r)}{\kappa r}, \tag{8.4}$$

with

$$\lambda = \frac{\beta' D'(\kappa\cosh\kappa - \sinh\kappa)}{(1+\beta')D'\kappa\cosh\kappa + (\beta' - D' - \beta' D')\sinh\kappa}. \tag{8.5}$$

As in Magar *et al.* (2003) we see that λ needs to be positive for the concentration at the surface to be smaller than the ambient concentration, and this is true for all (positive) values of the physical constants κ, β', D'. The Sherwood number is defined by equation (2.3), with a factor $1/(2\lambda)$ so that $Sh = 1$ at zero $1/\gamma$. The first-order (in ϵ) solution can be determined easily as well. However, we are only interested in the spherically symmetric term (that is the one proportional to P_0, which is independent of the angular direction) of the subsequent C_{0n} terms of the regular expansion, because that is the only one contributing to the integral in (2.3), and thus to the mass transfer. A series of computations lead us to a Sherwood number expansion of the form

$$Sh = 1 - \frac{\beta'}{\gamma} + O(\epsilon^2). \tag{8.6}$$

The Sherwood number is again – cf. equation (4.1) – a linear function of the Péclet number, up to this order; however, the slope does not depend on the streaming velocity but on the permeability of the membrane and the nutrient diffusivity. A decrease of nutrient diffusivity inside the cell leads to a decrease in nutrient absorption, while a decrease in membrane permeability has the opposite effect.

As for the large-$1/\gamma$ case, the analysis and the results are, qualitatively, the same as those presented in Magar *et al.* (2003), and the reader is referred to that paper for further details. The conclusion is that, with this alternative formulation, the Sherwood number is again of order one, that is, independent of the cell size, but still considerably larger than its value at $1/\gamma = 0$.

9. Conclusions

This study shows that the average nutrient uptake of an active squirmer depends on the propulsion mechanism, although either an increase in streaming speed or an increase in hovering speed enhances the uptake rate. We have concentrated on the

https://doi.org/10.1017/S0022112005005768 Published online by Cambridge University Press

case when the Péclet number is large, so that advection dominates the distribution of nutrients; the Sherwood number was expressed as an asymptotic solution for small and large values of the parameter $1/\gamma = \epsilon^2 P$.

Numerical and analytical solutions agree well when $1/\gamma$ is small, but some discrepancy appears at large $1/\gamma$, especially when streaming is present. We suggest that this is due to the small recirculation regions in the effective mean velocity field on the squirmer's surface: these regions are so small that the large-$1/\gamma$ asymptotic expansion could be valid only at immense values of $1/\gamma$, much larger than those presented in this paper. Also, a model of the average nutrient uptake, where we take into account consumption and diffusion inside the swimmer, led to results similar to those presented by Magar *et al.* (2003) for steady squirmers.

We have shown that there are optimal swimming characteristics for minimizing the energy dissipation for a given rate of nutrient uptake, at least for low and high values of the parameter $1/\gamma$. In particular, at large $1/\gamma$ hovering is energetically expensive, so pure streaming locomotion is likely to be observed. However, other propulsion mechanisms would come into play in special circumstances where the priorities of the micro-organism change from feeding to, for instance, surviving predation, or mating. In those cases, bursts of movement may be more appropriate and thus minimal energy criteria would be violated; however, during those bursts the absorption of nutrients could be very large.

Finally, we note that the model presented here is still too idealized to be applicable to any real living creature, so theoretical and experimental developments are still needed. As an example, radial oscillations of the surface of the swimmer are an important feature of any realistic model of ciliary propulsion, and should be included in models focusing on ciliate nutrient uptake. Also, it is of interest to analyse the sensitivity of the nutrient uptake to the choice of boundary conditions at the cell surface, when the squirmers are submerged in the turbulent ambient flows commonly encountered in the ocean.

We thank Dr T. Goto for providing the Finite Volume code and Dr J. Malarkey for his helpful comments on the final draft of the manuscript. This work was funded by a PhD grant from DGAPA (UNAM, Mexico) and a postdoctoral contract (from the University of Cambridge) to the first author. This is contribution 504/40 to the EU ELOISE NTAP project, number EVK-3-CT-2000-00022.

Appendix A. Explicit form of the velocity field

As explained in § 1, one can determine the explicit dependence on time and the three parameters b_1, b_2 and b_3 of the flow field, obtaining the expression (1.6) for the radial component, and expression (1.7) for the angular one. The functions in those equations are given by

$$u_0 = \frac{4b_2}{15}\left(\frac{3b_3}{7} - b_1\right)\left(\frac{1}{r^3} - 1\right)P_1 + \frac{b_2}{5}\left(2b_1 + \frac{b_3}{3}\right)\left(\frac{1}{r^5} - \frac{1}{r^3}\right)P_3, \tag{A 1}$$

$$u_1 = \frac{2}{3}b_1\left(\frac{1}{r^3} - 1\right)P_1\cos t - b_2\left(\frac{1}{r^4} - \frac{1}{r^2}\right)P_2\sin t + b_3\left(\frac{1}{r^5} - \frac{1}{r^3}\right)P_3\cos t, \tag{A 2}$$

$$u_2 = \frac{2b_2}{15}\left(b_1 + \frac{2b_3}{7}\right)\left(\frac{1}{r^3} - 1\right)P_1\cos 2t - \left(\frac{b_1^2}{2} - \frac{3b_1b_3}{7} + \frac{b_2^2}{14} - \frac{b_3^2}{28}\right)\left(\frac{1}{r^4} - \frac{1}{r^2}\right)P_2$$
$$\times \sin 2t + \frac{2b_2}{5}\left(\frac{b_3}{3} - 3b_1\right)\left(\frac{1}{r^5} - \frac{1}{r^3}\right)P_3\cos 2t, \tag{A 3}$$

https://doi.org/10.1017/S0022112005005768 Published online by Cambridge University Press

for the radial velocity, and

$$v_0 = \frac{4b_2}{15}\left(\frac{3b_3}{7} - b_1\right)\left(\frac{1}{2r^3} + 1\right)V_1 + \frac{b_2}{5}\left(2b_1 + \frac{b_3}{3}\right)\left(\frac{3}{2r^5} - \frac{1}{2r^3}\right)V_3, \tag{A 4}$$

$$v_1 = \frac{2}{3}b_1\left(\frac{1}{2r^3} + 1\right)V_1\cos t - b_2\frac{1}{r^4}V_2\sin t + b_3\left(\frac{3}{2r^5} - \frac{1}{2r^3}\right)V_3\cos t, \tag{A 5}$$

$$v_2 = \frac{2b_2}{15}\left(b_1 + \frac{2b_3}{7}\right)\left(\frac{1}{2r^3} + 1\right)V_1\cos 2t - \left(\frac{b_1^2}{2} - \frac{3b_1b_3}{7} + \frac{b_2^2}{14} - \frac{b_3^2}{28}\right)\frac{1}{r^4}V_2\sin 2t + \frac{2b_2}{5}\left(\frac{b_3}{3} - 3b_1\right)\left(\frac{3}{2r^5} - \frac{1}{2r^3}\right)V_3\cos 2t, \tag{A 6}$$

for the angular one. The functions above, when introduced in (1.6) and in (1.7), complete the determination of the flow field for the problem of the unsteady squirmer. Now, the velocity field can be written as

$$(u_j, v_j) = \mathrm{Re}(\tilde{\boldsymbol{u}}_j \exp(\mathrm{i}jt) = (\hat{u}_j, \hat{v}_j)\cos jt - (\tilde{u}_j, \tilde{v}_j)\sin jt.$$

From the equations above, it is easy to deduce that

$$(\hat{u}_0, \hat{v}_0) = (u_0, v_0); (\tilde{u}_0, \tilde{v}_0) = (0, 0);$$

$$(\hat{u}_1, \hat{v}_1) = \left[\frac{2}{3}b_1\left(\frac{1}{r^3} - 1\right)P_1 + b_3\left(\frac{1}{r^5} - \frac{1}{r^3}\right)P_3,\ \frac{2}{3}b_1\left(\frac{1}{2r^3} + 1\right)V_1 + b_3\left(\frac{3}{2r^5} - \frac{1}{2r^3}\right)V_3\right];$$

$$(\tilde{u}_1, \tilde{v}_1) = \left[b_2\left(\frac{1}{r^4} - \frac{1}{r^2}\right)P_2,\ b_2\frac{1}{r^4}V_2\right];$$

$$\hat{u}_2 = \frac{2b_2}{15}\left(b_1 + \frac{2b_3}{7}\right)\left(\frac{1}{r^3} - 1\right)P_1 + \frac{2b_2}{5}\left(\frac{b_3}{3} - 3b_1\right)\left(\frac{1}{r^5} - \frac{1}{r^3}\right)P_3;$$

$$\hat{v}_2 = \frac{2b_2}{15}\left(b_1 + \frac{2b_3}{7}\right)\left(\frac{1}{2r^3} + 1\right)V_1 + \frac{2b_2}{5}\left(\frac{b_3}{3} - 3b_1\right)\left(\frac{3}{2r^5} - \frac{1}{2r^3}\right)V_3;$$

$$(\tilde{u}_2, \tilde{v}_2) = \left[\left(\frac{b_1^2}{2} - \frac{3b_1b_3}{7} + \frac{b_2^2}{14} - \frac{b_3^2}{28}\right)\left(\frac{1}{r^4} - \frac{1}{r^2}\right)P_2,\ \left(\frac{b_1^2}{2} - \frac{3b_1b_3}{7} + \frac{b_2^2}{14} - \frac{b_3^2}{28}\right)\frac{1}{r^4}V_2\right].$$

Also, in order to determine the concentration field, we need to consider an approximation of the velocity near the surface of the micro-organism. We accomplish this by performing a Taylor expansion of the expressions for (u_j, v_j), around $r = 1$; we scale the layer close to the surface by ϵ, so that the coordinate Y perpendicular to the surface is defined as $\epsilon Y = r - 1$. Then we deduce that the radial velocity may be written as $(u_0, u_1, u_2) = \epsilon Y(u_{01}, u_{11}, u_{21}) + O(\epsilon^2 Y^2)$, and the angular component as $(v_0, v_1, v_2) = (v_{00}, v_{10}, v_{20}) + \epsilon Y(v_{01}, v_{11}, v_{21}) + O(\epsilon^2 Y^2)$, with each of the terms as follows:

$$u_{01} = -2\left[\left(\frac{6b_2b_3}{35} - \frac{2b_1b_2}{5}\right)P_1 + \left(\frac{2b_1b_2}{5} + \frac{b_2b_3}{15}\right)P_3\right],$$

$$u_{11} = -2[(b_1P_1 + b_3P_3)\cos t - b_2P_2\sin t],$$

$$u_{21} = -2\left[\left(\frac{b_1b_2}{5} + \frac{2b_2b_3}{35}\right)P_1 + \left(\frac{2b_2b_3}{15} - \frac{6b_1b_2}{5}\right)P_3\right]\cos 2t + 2\left(\frac{b_1^2}{2} - \frac{3b_1b_3}{7} + \frac{b_2^2}{14} - \frac{b_3^2}{28}\right)P_2\sin 2t,$$

$$v_{00} = \left(\frac{6b_2b_3}{35} - \frac{2b_1b_2}{5}\right)V_1 + \left(\frac{2b_1b_2}{5} + \frac{b_2b_3}{15}\right)V_3,$$

https://doi.org/10.1017/S0022112005005768 Published online by Cambridge University Press

$$v_{10} = (b_1V_1 + b_3V_3)\cos t - b_2V_2 \sin t,$$
$$v_{20} = \left[\left(\frac{b_1b_2}{5} + \frac{2b_2b_3}{35}\right)V_1 + \left(\frac{2b_2b_3}{15} - \frac{6b_1b_2}{5}\right)V_3\right]\cos 2t$$
$$-\left(\frac{b_1^2}{2} - \frac{3b_1b_3}{7} + \frac{b_2^2}{14} - \frac{b_3^2}{28}\right)V_2 \sin 2t,$$
$$v_{01} = -\left(\frac{6b_2b_3}{35} - \frac{2b_1b_2}{5}\right)V_1 - 6\left(\frac{2b_1b_2}{5} + \frac{b_2b_3}{15}\right)V_3,$$
$$v_{11} = (-b_1V_1 - 6b_3V_3)\cos t + 4b_2V_2 \sin t,$$
$$v_{21} = \left[-\left(\frac{b_1b_2}{5} + \frac{2b_2b_3}{35}\right)V_1 - 6\left(\frac{2b_2b_3}{15} - \frac{6b_1b_2}{5}\right)V_3\right]\cos 2t$$
$$+ 4\left(\frac{b_1^2}{2} - \frac{3b_1b_3}{7} + \frac{b_2^2}{14} - \frac{b_3^2}{28}\right)V_2 \sin 2t.$$

Appendix B. Calculation of the effective velocity field

Introducing the velocity field defined in (3.6) into the transport equation (3.5), we first note that

$$\text{Im}\,(\tilde{\boldsymbol{u}}_1 \cdot \nabla\bar{\tilde{\boldsymbol{u}}}_1)\cdot\nabla C_0 = \left[\tilde{u}_1\frac{\partial}{\partial r}\hat{u}_1 - \hat{u}_1\frac{\partial}{\partial r}\tilde{u}_1 + \frac{1}{r}\left(\tilde{v}_1\frac{\partial}{\partial\theta}\hat{u}_1 - \hat{v}_1\frac{\partial}{\partial\theta}\tilde{u}_1\right)\right]\frac{\partial C_0}{\partial r}$$
$$+\left[\tilde{u}_1\frac{\partial}{\partial r}\hat{v}_1 - \hat{u}_1\frac{\partial}{\partial r}\tilde{v}_1 + \frac{1}{r}\left(\tilde{v}_1\frac{\partial}{\partial\theta}\hat{v}_1 - \hat{v}_1\frac{\partial}{\partial\theta}\tilde{v}_1\right)\right]\left(\frac{1}{r}\frac{\partial C_0}{\partial\theta}\right),$$

where the operators in the square brackets apply to the product of the velocity component on their bigg and the corresponding component of the concentration gradient. Equation (3.5) may, thus, be written as

$$(A_{r1} + u_0)\frac{\partial C_0}{\partial r} + \frac{A_{\theta 1} + v_0}{r}\frac{\partial C_0}{\partial\theta} = \gamma\nabla^2 C_0.$$

Therefore, the contribution to the effective velocity field, due to the flow (u_1, v_1), is of the form

$$A_{r1} = \frac{1}{2}\left\{\tilde{u}_1(\hat{u}_1)_r - \hat{u}_1(\tilde{u}_1)_r + \frac{1}{r}[\tilde{v}_1(\hat{u}_1)_\theta - \hat{v}_1(\tilde{u}_1)_\theta]\right\},$$
$$A_{\theta 1} = \frac{1}{2}\left\{\tilde{u}_1(\hat{v}_1)_r - \hat{u}_1(\tilde{v}_1)_r + \frac{1}{r}[\tilde{v}_1(\hat{v}_1)_\theta - \hat{v}_1(\tilde{v}_1)_\theta + \hat{u}_1\tilde{v}_1 - \tilde{u}_1\hat{v}_1]\right\},$$

where the subscript following a round bracket means partial differentiation, with respect to that subscript, of the velocity component inside the round brackets. All the spatial functions $\tilde{u}_1$, $\hat{u}_1$, $\tilde{v}_1$, $\hat{v}_1$, and their derivatives, may be easily deduced from the definitions in Appendix A and from simple algebraic manipulations. We now replace the terms by their explicit form as functions of r, the Legendre polynomials, and their derivatives. Then we write both $(A_{r1}, A_{\theta 1})$ and (u_0, v_0) as sine and cosine series, and sum the series. We obtain (A_r, A_θ) as a Fourier expansion. The final step is to write each sine and cosine as a sum of Legendre polynomials (for A_r), or as a sum of the polynomials V_n (for A_θ). The resulting expressions are, then, manipulated so that the effective velocity can be represented as the sum of a *hovering* velocity, $(\boldsymbol{A})_{\text{hov}}$, which is proportional to the parameter $b = b_1b_2$, and a *streaming* velocity vector, $(\boldsymbol{A})_{\text{unif}}$,

https://doi.org/10.1017/S0022112005005768 Published online by Cambridge University Press

proportional to the velocity scale W we defined as

$$W = \frac{4}{5}b_2\left(-\frac{b_1}{3}+\frac{b_3}{7}\right).$$

Thus, the velocity field is written as $A_r = b(A_r)_{\mathrm{hov}} + W(A_r)_{\mathrm{unif}}$, and $A_\theta = (A_\theta)_{\mathrm{hov}} + (A_\theta)_{\mathrm{unif}}$, and its components are as follows:

$$\begin{aligned}(A_r)_{\mathrm{hov}} = {} & P_1\left(-\frac{2}{15r^3}-\frac{1}{6r^6}+\frac{4}{5r^8}-\frac{1}{2r^{10}}\right)\\ & + P_3\left(\frac{11}{45r^3}-\frac{7}{9r^5}+\frac{1}{6r^6}+\frac{34}{45r^8}-\frac{7}{18r^{10}}\right)\\ & + P_5\left(-\frac{5}{6r^6}+\frac{10}{9r^8}-\frac{5}{18r^{10}}\right),\end{aligned} \tag{B 1}$$

$$\begin{aligned}(A_\theta)_{\mathrm{hov}} = {} & V_1\left(-\frac{1}{15r^3}-\frac{1}{3r^6}+\frac{12}{5r^8}-\frac{2}{r^{10}}\right)\\ & + V_3\left(\frac{11}{90r^3}-\frac{7}{6r^5}+\frac{1}{3r^6}+\frac{34}{15r^8}-\frac{14}{9r^{10}}\right)\\ & - V_5\left(\frac{5}{3r^6}-\frac{10}{3r^8}+\frac{10}{9r^{10}}\right),\end{aligned} \tag{B 2}$$

$$\begin{aligned}(A_r)_{\mathrm{unif}} = {} & P_1\left(-1+\frac{1}{r^3}-\frac{3}{8r^6}+\frac{9}{4r^8}-\frac{15}{8r^{10}}\right)\\ & + P_3\left(-\frac{7}{12r^3}+\frac{7}{12r^5}-\frac{7}{8r^6}+\frac{7}{3r^8}-\frac{35}{24r^{10}}\right)\\ & + P_5\left(-\frac{25}{8r^6}+\frac{25}{6r^8}-\frac{25}{24r^{10}}\right),\end{aligned} \tag{B 3}$$

$$\begin{aligned}(A_\theta)_{\mathrm{unif}} = {} & V_1\left(1+\frac{1}{2r^3}-\frac{3}{4r^6}+\frac{27}{4r^8}-\frac{15}{2r^{10}}\right)\\ & + V_3\left(-\frac{7}{24r^3}+\frac{7}{8r^5}-\frac{7}{4r^6}+\frac{7}{r^8}-\frac{35}{6r^{10}}\right)\\ & - V_5\left(\frac{25}{4r^6}-\frac{25}{2r^8}+\frac{25}{6r^{10}}\right).\end{aligned} \tag{B 4}$$

Notice that the tangential velocity at the surface of the micro-organism is $5(b/3 + W/4)V_5$, and thus vanishes at the same points as V_5.

Also, it can be easily shown that the velocity field above is solenoidal, and that it is the gradient of a stream function $\psi = b\,\psi_{\mathrm{hov}} + W\,\psi_{\mathrm{unif}}$, where

$$\begin{aligned}\psi_{\mathrm{hov}} = {} & \sin^2\theta\left(-\frac{1}{15r}-\frac{1}{12r^4}+\frac{2}{5r^6}-\frac{1}{4r^8}\right)\\ & + \left(-\frac{5}{4}\cos^4\theta+\frac{3}{2}\cos^2\theta-\frac{1}{4}\right)\left(\frac{11}{90r}-\frac{7}{18r^3}+\frac{1}{12r^4}+\frac{17}{45r^6}-\frac{7}{36r^8}\right)\\ & + \left(-\frac{21}{8}\cos^6\theta+\frac{35}{8}\cos^4\theta-\frac{15}{8}\cos^2\theta+\frac{1}{8}\right)\left(-\frac{5}{12r^4}+\frac{5}{9r^6}-\frac{5}{36r^8}\right),\end{aligned}$$

https://doi.org/10.1017/S0022112005005768 Published online by Cambridge University Press

and

$$\psi_{\text{unif}} = \sin^2\theta\left(-\frac{r^2}{2}+\frac{1}{2r}-\frac{3}{16r^4}+\frac{9}{8r^6}-\frac{15}{16r^8}\right)$$
$$+\left(-\frac{5}{4}\cos^4\theta+\frac{3}{2}\cos^2\theta-\frac{1}{4}\right)\left(-\frac{7}{24r}+\frac{7}{24r^3}-\frac{7}{16r^4}+\frac{7}{6r^6}-\frac{35}{48r^8}\right)$$
$$+\left(-\frac{21}{8}\cos^6\theta+\frac{35}{8}\cos^4\theta-\frac{15}{8}\cos^2\theta+\frac{1}{8}\right)\left(-\frac{25}{16r^4}+\frac{25}{12r^6}-\frac{25}{48r^8}\right),$$

are the hovering and the streaming stream functions, respectively.

REFERENCES

Acrivos, A. & Taylor, T. D. 1962 Heat and mass transfer from single spheres in Stokes flow. *Phys. Fluids* **5**, 387–394.

Blake, J. R. 1971*a* Infinite models for ciliary propulsion. *J. Fluid Mech.* **49**, 209–222.

Blake, J. R. 1971*b* A spherical envelope approach to ciliary propulsion. *J. Fluid Mech.* **46**, 199–208.

Blom, J. G., Trompert, R. A. & Verwer, J. G. 1996 Algorithm 758: VLUGR2: A vectorizable adpative grid solver for PDEs in 2D. *ACM Trans. Math. Softw.* **22**, 302–328.

Brennen, C. 1974 An oscillatory-boundary-layer theory for ciliary propulsion. *J. Fluid Mech.* **65**, 799–824.

Crawford, D. W. 1989 Mesodinium rubrum: the phytoplankter that wasn't. *Marine Ecology Progress Series* **58**, 161–174.

Crawford, D. W. 1992 Metabolic cost of motility in planktonic protists: Theoretical considerations on size scaling and swimming speed. *Microbial Ecology* **24**, 1–10.

Crawford, D. W. & Purdie, D. A. 1992 Evidence for avoidance of flushing from an estuary by a planktonic, phototrophic ciliate. *Marine Ecology Progress Series* **79**, 259–265.

Dale, T. 1987 Diel vertical distribution of planktonic ciliates in lindaspollene, western norway. *Marine Microbial Food Webs* **2**, 15–28.

Ehlers, K. M., Samuel, A. D. T., Berg, H. C. & Montgomery, R. 1996 Do cyanobacteria swim using traveling surface waves? *Proc. Natl Acad. Sci. USA* **93**, 8340–8343.

Ghiu, S. M. S., Carnahan, R. P. & Barger, M. 2002 Permeability of electrolytes through a flat RO membrane in a direct osmosis study. *Desalination* **144** (1-3), 387–392.

Hoiczyk, E. 2000 Gliding motility in cyanobacteria: observations and possible explanations. *Arch. Microbiol.* **174**, 11–17.

Hoiczyk, E. & Baumeister, W. 1995 Envelope structure of four gliding filamentous cyanobacteria. *J. Bacteriol.* **177**, 2387–2395.

Jakobsen, H. 2001 Escape response of planktonic protists to fluid mechanical signals. *Mar. Ecol. Prog. Ser.* **214**, 67–78.

Koehl, M. A. R. 1989 Discussion: From Individuals to Populations. In *Perspectives in Ecological Theory* (ed. J. Roughgarden, R. M. May & S. A. Levin), chap. 3, pp. 39–53. Princeton University Press.

Krainer, K. H. & Foissner, W. 1990 Revision of the Genus Askenasia Blochmann, 1895, with proposal of two new species, and description of Rhabdoaskenasia minima n. g, n. sp. (Cilophora, Cyclotrichida). *J. Protozool.* **37**, 414–427.

Leal, L. G. 1992 *Laminar Flow and Convective Transport Processes: Scaling Principles and Asymptotic Analysis*. Butterworth-Heinemann.

Lighthill, M. J. 1952 On the squirming motion of nearly spherical deformable bodies through liquids at very small Reynolds numbers. *Commun. Pure Appl. Maths* **5**, 109–118.

Magar, V., Goto, T. & Pedley, T. J. 2003 Nutrient uptake by a self-propelled steady squirmer. *Q. J. Mech. Appl. Maths* **56**, 65–91.

Saad, Y. & Schultz, M. H. 1986 GMRES: a generalized minimal residual algorithm for solving nonsymmetric linear systems. *SIAM J. Sci. Statist. Comput.* **7**, 856–869.

Samuel, A. D. T., Petersen, J. D. & Reese, T. S. 2001 Envelope structure of *Synechococcus* sp. WH8113, a nonflagellated swimming cyanobacterium. *BMC Microbiology* **1**, 1–4.

https://doi.org/10.1017/S0022112005005768 Published online by Cambridge University Press

Skerker, J. M. & Berg, H. C. 2001 Direct observation of extension and retraction of type IV pili. *Proc. Natl Acad. Sci. USA* **98**, 6901–6904.

Sleigh, M. A. & Blake, J. R. 1977 Methods of ciliary propulsion and their size limitations. In *Scale Effects in Animal Locomotion Based on the Proceedings of an International Symposium held at Cambridge University, September 1975* (ed. T. J. Pedley), pp. 79–92. Academic.

Stone, H. A. & Samuel, A. D. T. 1996 Propulsion of micro-organisms by surface distortions. *Phys. Rev. Let*. **77**, 4102–4104.

Taylor, G. I. 1951 Analysis of the swimming of microscopic organisms. *Proc. R. Soc. Lond*. A **211**, 225–239.

Tuck, E. O. 1968 a note on a swimming problem. *J. Fluid Mech*. **31**, 305–308.

Wall, D. & Kaiser, D. 1999 Type IV pili and cell motility. *Mol. Microbiol*. **32**, 1–10.

https://doi.org/10.1017/S0022112005005768 Published online by Cambridge University Press